Journal of Materials Chemistry C

RSC Publishing

PAPER

View Article Online
View Journal | View Issue

Published on 24 September 2013. Downloaded by HK University of Science and Technology on 01/09/2017 07:53:27.

Cite this: J. Mater. Chem. C, 2013, 1, 7314

Defect-sensitive crystals based on diaminomaleonitrile-functionalized Schiff base with aggregation-enhanced emission†

Tianyu Han,[ab] Yuning Hong,[a] Ni Xie,[a] Sijie Chen,[a] Na Zhao,[a] Engui Zhao,[a] Jacky W. Y. Lam,[a] Herman H. Y. Sung,[a] Yuping Dong,[b] Bin Tong*[b] and Ben Zhong Tang*[acd]

Received 9th August 2013
Accepted 20th September 2013

DOI: 10.1039/c3tc31562b

www.rsc.org/MaterialsC

In this work, we report the synthesis and photophysical studies of a new luminogen, A3MN, a diaminomaleonitrile-functionalized Schiff base. A3MN is aggregation-enhanced emission (AEE)-active: the emission of A3MN is enhanced with the aggregate formation. A3MN also possesses twisted intramolecular charge transfer (TICT) properties, showing noticeable solvatofluorochromism. Interestingly, the crystals of A3MN are nonemissive; the defect areas of the crystal, however, are highly emissive, as confirmed by spectroscopic methods and confocal microscopy. By taking advantage of this defect sensitive feature, a "turn-on" type of mechanofluorochromic material is developed, the emission of which is significantly enhanced under pressure or shear force. The detection limit reaches 0.1 Newton owing to its "turn-on" nature. Such defect-induced emission also renders A3MN sensitive to various kinds of mechanical actions, including hitting, friction, sculpture, and ultrasonic vibration.

Introduction

Conventional fluorescent molecules, such as pyrene and perylene, typically consist of large planar aromatic rings, which easily undergo intermolecular π–π interactions in the aggregate state. The close vicinity of these chromophores often induces non-radiative energy transfer resulting in drastic reduction of the luminescence signals [aggregation-caused quenching (ACQ)], which greatly limits their applications as efficient light-emitting materials or sensors.[1–3] To alleviate the ACQ effect, various chemical, physical and engineering approaches have been developed to interfere with the aggregation of the luminogens.[4] The attempts, however, have met with only limited success because aggregation is a natural process when the dye molecules are located in close proximity in the condensed phase.

The emergence of luminogens with aggregation-induced emission (AIE) or aggregation-enhanced emission (AEE) characteristics can circumvent the ACQ problem.[5] These propeller-shaped luminogens including small molecules and polymers are non-emissive or weakly emissive in dilute solutions but emit efficiently upon aggregate formation. Through experimental and theoretical studies, restriction of intramolecular motions (RIM) is proposed as the mechanism for the AIE/AEE effect.[6] Since the discovery of this novel phenomenon in 2001, many research efforts have been made and oriented to the exploration of their applications, including as excellent emitters for the fabrication of efficient organic light-emitting diodes (OLED) and sensitive environmental and biological probes.[7]

To expand the scope of the AIE/AEE systems for biomedical and other high-tech applications, especially for *in vivo* imaging, fluorescent probes with intense emission in the red/near infrared regions are highly desired.[8] Although many AIE/AEE systems [*e.g.* silole,[5] tetraphenylethene (TPE),[9] dihydrocyclopentaindene derivatives,[10] dibenzosubereneanthracene derivatives,[11] styrylpyridinium derivatives,[12] phosphole derivatives,[13] benzobis(thiadiazole) derivatives,[14] aryl-substituted pyrrole derivatives,[15] *etc.*] have been developed, most of them emit blue or green light. To red-shift the emission colors of the luminogens, generally there are two major approaches. One is increasing the conformational planarity and electronic conjugation. This approach, however, will also increase intermolecular π–π interactions and promote the formation of detrimental species as excimers and

[a]Department of Chemistry, Institute for Advanced Study, State Key Laboratory of Molecular Neuroscience, Institute of Molecular Functional Materials and Division of Biomedical Engineering, The Hong Kong University of Science & Technology (HKUST), Clear Water Bay, Kowloon, Hong Kong, China. E-mail: tangbenz@ust.hk; Fax: +852 23581594

[b]College of Materials Science and Engineering, Beijing Institute of Technology, 5 South Zhongguancun Street, Beijing, 100081, China. E-mail: tongbin@bit.edu.cn; Fax: +86-10-6894-8982

[c]Guangdong Innovative Research Team, SCUT-HKUST Joint Research 50 Laboratory, State Key Laboratory of Luminescent Materials and Devices, South China University of Technology (SCUT), Guangzhou 510640, China

[d]HKUST Shenzhen Research Institute, No. 9 Yuexing 1st RD, South Area, Hi-tech Park, Nanshan, Shenzhen 518057, China

† Electronic supplementary information (ESI) available: Synthesis and characterization, particle size analysis, fluorescence lifetime and crystal data for A3MN. For ESI and crystallographic data in CIF, video or other electronic formats see DOI: 10.1039/c3tc31562b

This journal is © The Royal Society of Chemistry 2013

Published on 24 September 2013. Downloaded by HK University of Science and Technology on 01/09/2017 07:53:27.

exciplexes, resulting in the undesired ACQ effect. The other approach is incorporating electron donor (D) and acceptor (A) pairs to induce intramolecular charge transfer (ICT) in order to lower the π–π* energy gap and consequently a large bathochromic shift in the emission color.[16] A fusion of the AIE and ICT may create luminogens with long emission color while overcoming the severe ACQ problem encountered by traditional D–π–A structured ICT systems.

In search of the current AIE/AEE systems, silole and TPE are the archetypes. Siloles are extremely bright emitters in the aggregate state. Structural modification of siloles, however, requires a troublesome and tedious synthetic process, setting a big obstacle on their industrialization for real-world applications. In contrast, AIE/AEE luminogens which are easily accessible and ready to functionalize tend to be widely and constantly used for different applications. For example, TPE, which can be simply synthesized through one-step McMurry coupling of benzophenone, becomes a "star" of AIE molecules whose derivatives have been utilized in many areas.[17] Although we have previously incorporated the ICT system into TPE to generate long-wavelength emitting AIE molecules, the resulting luminogens are generally bulky and require further physical modification to exert their functions. Furthermore, the strong fluorescence of the existing AIE/AEE systems in the solid state, though beneficial for OLED and bioimaging, is sort of a hindrance when developing solid-state sensing platforms which require both low background noise and high "off/on" ratio. Solid-state sensing systems are more desirable because they can be easily fabricated into portable devices for simple and rapid on-site detection.[18] Although the solid state of AIE/AEE molecules has been used for sensing explosives, gases and mechanical forces through fluorescence "turn-off",[19] people prefer "turn-on" sensing mode as it is more sensitive and less likely to generate false-positive signals than its "turn-off" counterparts.[20] Unfortunately, it is difficult to suppress the emission of AIE/AEE molecules in the solid state owing to their nature. Therefore, it is an urgent and important task to explore a new AIE/AEE system with easy synthetic accessibility and switchable solid-state emission.[21]

In this paper, we present a brand new AEE system fulfilling these two criteria. 2-Amino-3-((*E*)-(4-(diethylamino)benzylidene) amino)maleonitrile (A3MN) was facilely synthesized by a one-step reaction. Due to the electron donating (diethylamino) and withdrawing (cyano) moieties, it exhibits solvatochromism and strong emission at a long-wavelength of 563 nm in the aggregate state. Interestingly, we found that the intact crystals of A3MN are weakly emissive while the defect areas of the crystals are highly luminescent. Based on this unique defect-sensitive property, we investigated the emission of A3MN crystals induced by solvent etching, mechanical force as well as exposure to ultrasonic vibration.

Results and discussion

Synthesis and structural characterization

A3MN was synthesized by a simple one-step reaction shown in Scheme 1. The reaction was conducted under mild conditions, affording a good yield of 83.1%. The product was fully characterized by spectroscopic methods from which satisfactory analysis data were obtained. The detailed synthetic procedure and characterization data are available in the ESI.† Single crystals of A3MN were grown from a THF–ethanol mixture and analysed by X-ray diffraction crystallography. The crystal structure of A3MN is displayed in the inset of Scheme 1, which reveals that the C=N bond is in *trans*-conformation. Detailed crystal data are given in Tables S1 and S2 (ESI).† A3MN is soluble in common organic solvents such as chloroform, THF, acetone, ethyl acetate and DMSO, slightly soluble in methanol, and completely insoluble in water.

Solvatochromism

The broad-range solubility of A3MN allows us to investigate its photophysical properties in the solvents with varying polarities. UV-visible spectra show that the absorption peaks appear at around 430 nm, corresponding to the π–π* transition of A3MN. With an increase in the solvent polarity, the absorption maximum of A3MN slightly red-shifts from 425 to 438 nm (Fig. 1A). When excited at 440 nm, the solutions of A3MN emit weakly in the blue region in low-polar solvents such as chloroform and toluene, while in relatively polar solvents such as acetone and DMSO, the emission colour is red-shifted to yellow (Fig. 1B). A drastic bathochromic shift of the emission maximum is recorded from 468 to 514 nm (Fig. 1B).

The solvatochromism of A3MN can be explained by the twisted intramolecular charge transfer (TICT) mechanism.[16] Just like most of the TICT molecules, A3MN is comprised of D and A units, resulting in large molecular dipoles and an asymmetric electron population in the frontier molecular orbitals (Fig. 2). The electron cloud in the HOMO level distributes over the whole molecule, while in the LUMO level the electron cloud mainly localizes on the maleonitrile moiety due to its strong electron-withdrawing effect. The difference in the electron distribution of the HOMO and LUMO results in a large energy gap of 3.224 eV, which is narrowed when the molecule is surrounded by polar solvents. According to the Franck–Condon principle, the molecule in the locally excited (LE) state is almost planar, while solvent relaxation occurs with the intramolecular rotation of the diethylamino group to a right angle in which the conjugation of the molecule is partially jeopardized. In the resulting TICT state, there is a total charge separation between

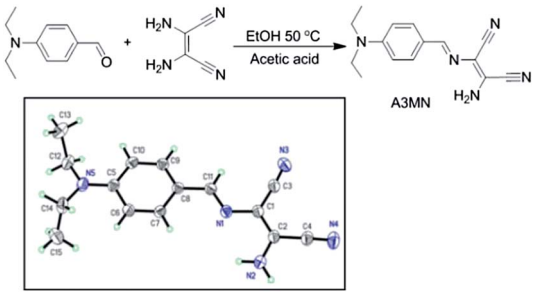

Scheme 1 Synthetic route to A3MN and the ORTEP drawing of its single crystal structure.

Published on 24 September 2013. Downloaded by HK University of Science and Technology on 01/09/2017 07:53:27.

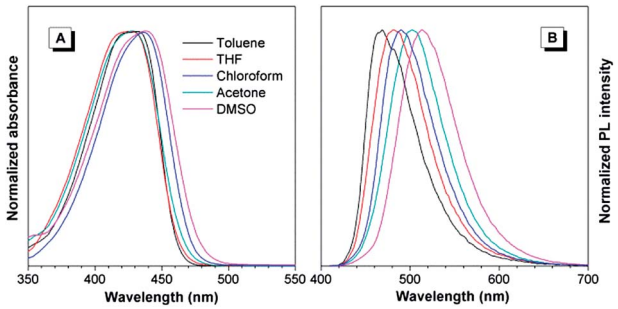

Fig. 1 (A) Absorption and (B) emission spectra of A3MN in different organic solvents. Concentration: 10 μM. Excitation wavelength: 400 nm.

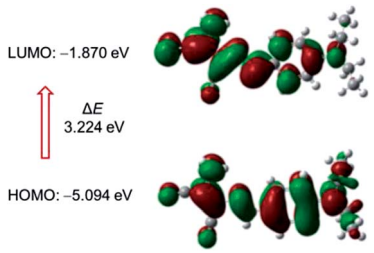

Fig. 2 Molecular orbital amplitude plots of HOMO and LUMO energy levels of A3MN calculated by using the B3LYP/6-31G basis set.

the D and A units which can be stabilized by the polar solvent molecules. The stabilization could thus reduce the LUMO energy level of the TICT state and consequently red-shift the absorption and emission bands.

Aggregation-enhanced emission

Some molecules fluoresce in the solution state and their fluorescence is further enhanced upon aggregate formation. We coined this as aggregation-enhanced emission (AEE).[17] The dilute THF solution of A3MN exhibits weak emission at ~480 nm when photoexcited at 445 nm (Fig. 3A). The emission is intensified and red-shifted when water, a poor solvent of A3MN, is added. In a THF–water mixture with 80 vol% of water, the fluorescence intensity is around 4-fold higher than that in pure THF solution, showing the AEE phenomenon (Fig. 3B). The aggregation formation is supported by particle size analysis *via* the dynamic light scattering (DLS) method. Fig. S4A† reveals the existence of particles with average sizes of *ca.* 280 and 208 nm in the THF–water mixture with 80 and 90% water fraction, respectively. Due to the space constraint in the aggregates, the intramolecular motions of the dye molecules will be restricted and the emission is thus enhanced. On the other hand, addition of water gradually shifts the emission maximum of A3MN to the longer wavelength region (Fig. 3B). The change in the spectral profile can be attributed to the TICT process due to the increase of solvent polarity upon addition of water.

Crystallization-caused quenching

The emission of A3MN is enhanced along with the increase of water fraction up to 80% in the solvent mixtures. Different from

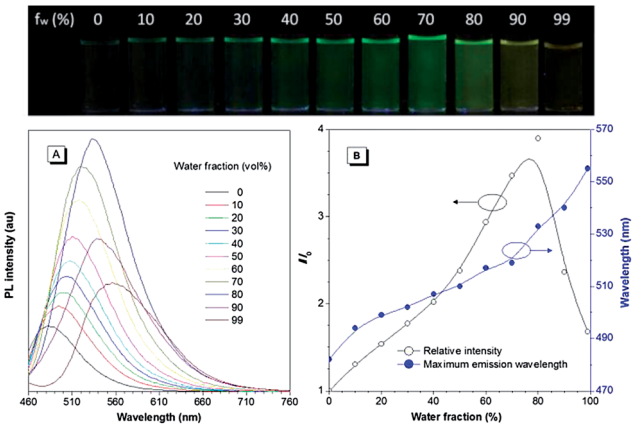

Fig. 3 (A) PL spectra of A3MN in THF and THF–water mixtures with different water fractions. Photographs of A3MN in different water fractions taken under UV illumination are shown in the upper panel. (B) Plots of the I/I_0 value and maximum emission wavelength *versus* the composition of the aqueous mixtures of A3MN. Concentration: 10 μM. Excitation wavelength: 445 nm.

many other AIE/AEE systems, further increasing the water fraction, however, leads to the decrease of the emission intensity (Fig. 3B). In a THF–water mixture with 99% water fraction, the emission is lower than that with 90% water. Moreover, we observed that the emission intensity of a freshly prepared sample with 99% water gradually decreases with time as depicted in Fig. 4, while the emission maximum remains almost unchanged. After ~35 min, the fluorescence of A3MN in 99% water reaches the lowest level and remains constant afterwards. The particle size of A3MN in 99% water reveals that large particles are formed with a diameter of *ca.* 1 μm (Fig. S4C†).

The time-dependent decrease of the fluorescence and the change of particle size of the aggregates imply that a recrystallization process might take place in 99% water fraction. To verify this hypothesis, transmission electron microscopy (TEM) is applied to examine the morphology of the aggregates. The freshly prepared aggregates show a chaotic structure with the size of around 200 nm that agrees well with the DLS measurement (Fig. 5A–D). Upon aging for 2 hours, the aggregates collected from the same sample grow into crystal-like structures at the micron scale with well-defined shape (Fig. 5E–H). We thus speculate that the crystallization of A3MN may quench the light emission.

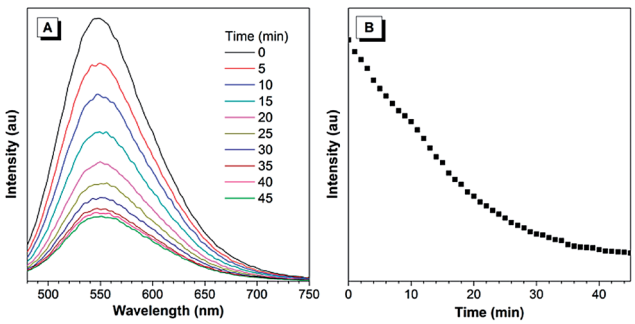

Fig. 4 (A) Time-dependent fluorescence spectra of A3MN in a THF–water mixture with 99% water fraction. (B) Plot of intensities *versus* time. Concentration: 10 μM. Excitation wavelength: 400 nm.

This journal is © The Royal Society of Chemistry 2013

Published on 24 September 2013. Downloaded by HK University of Science and Technology on 01/09/2017 07:53:27.

To understand how the molecular packing affects the emission behaviour of A3MN, a single crystal of A3MN is grown by slow evaporation of its THF–ethanol solution. The crystals, however, are weakly fluorescent with a solid-state quantum yield (Φ_F) of 3.77%, in accord with our above observation of the fluorescence decrease during the recrystallization process (see Fig. 4). We then look into the geometric structure and packing arrangements of A3MN crystals. Different from most of the propeller-shaped AIE/AEE molecules which have twisted conformations in the crystalline state, A3MN adopts a planar conformation in the crystal lattice with an interplanar spacing of around 3.382 nm. The aromatic ring and the central C=N bond together with the maleonitrile moiety are located on the same plane: the torsional angle between the benzene ring and the C=N moiety is 2.35° and the torsional angle between the C=N bond and the C=C moiety is merely 0.07° (Table S2†). As shown in Fig. 6A, the adjacent molecules align in an antiparallel packing mode owing to the D–A effect with the electron-withdrawing maleonitrile moiety pointing to the electron-donating diethylamine unit. Hydrogen bonding is formed between the NH_2 group and the C≡N bond on the adjacent molecule (Fig. 6B). From the top view, the C=C bond directly stacks on top of the phenyl ring of the neighbouring molecule with an intermolecular distance of 3.358 nm, within the range of intermolecular π–π stacking. The strong π–π interactions promote the decay of the excited species through nonradiative pathways, resulting in the weak fluorescence in A3MN crystals.

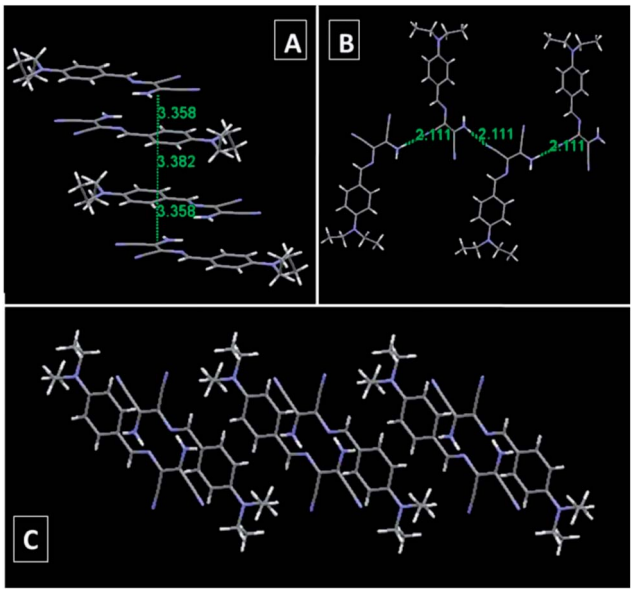

Fig. 6 Molecular packing showing (A) π–π interactions and (B) hydrogen bonding in the single crystal lattice of A3MN. (C) The top view of the molecular packing.

Defect-induced emission

Defect-related luminescent materials, in combination with their controllable and tunable behaviours, have aroused much attention in the recent decades, because of their potential applications in drug delivery, bioimaging, and even homeland security.[22] Initially, the nonemissive crystals of A3MN disappoint us. Luckily, we found that A3MN is a defect sensitive material: the defect area of the crystals becomes highly emissive. As shown in Fig. 7A, a pristine single crystal of A3MN is almost nonemissive when photoexcited at 405 nm under a fluorescence microscope. When etched by acetone for 1 s, the fluorescence of the crystal is turned on (Fig. 7B). Extending the etching time can further enhance the fluorescence (Fig. 7C). It is suggested that the acetone molecules may invade into the A3MN crystal lattice and partially dissolve the crystal. Simultaneously, there is not enough time for the dissolved molecules to stack closely and regularly by π–π interactions during fast acetone evaporation, leading to the formation of crystal defects at the etched area.

On the other hand, rupturing the A3MN crystal using a metal spatula can also form defects on the crystal. As expected, intense emission is observed in the fracture surface under a fluorescence microscope (Fig. 7D and E). Similarly, strong fluorescence is observed when the crystal is crushed (Fig. 7E and F).

The defect-induced emission is further confirmed using a confocal laser scanning microscope. The single crystal of A3MN is "dark" in most areas when excited at 405 nm (Fig. S5A†). The

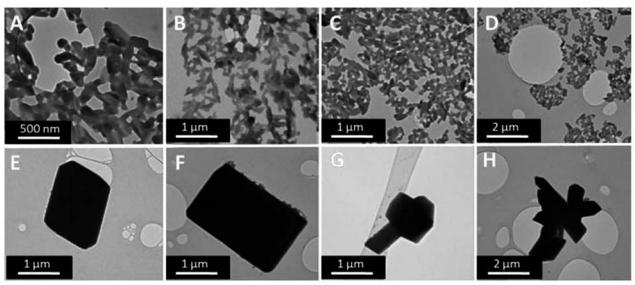

Fig. 5 (A–D) TEM images of A3MN aggregates collected immediately and (E–H) 2 h later after the addition of 99% water into the stock solution in THF. Concentration: 10 μM.

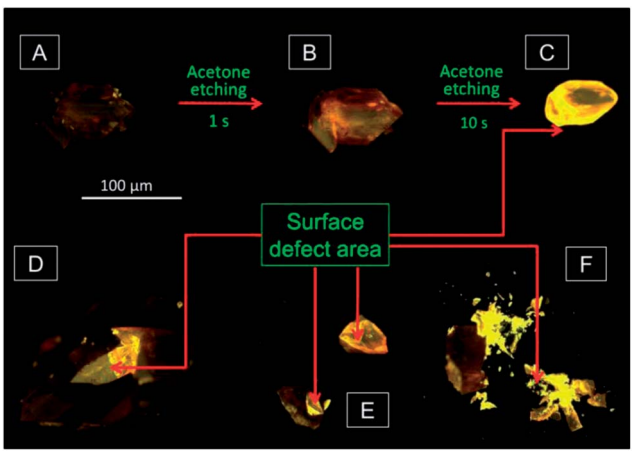

Fig. 7 Micrographs of single crystals of A3MN under UV irradiation: (A) pristine single crystal, (B and C) single crystal etched by acetone for (B) 1 and (C) 10 s, and (D–F) single crystal with surface defects.

Published on 24 September 2013. Downloaded by HK University of Science and Technology on 01/09/2017 07:53:27.

yellow-emission spots may be originated from the defect area which is naturally formed during crystal growth. Layer-by-layer scanning reveals that neither the interior nor the surface of the crystal is strongly fluorescent (Fig. S5C†). On the other hand, when etching with acetone, the surface of the crystal becomes highly emissive (Fig. S5B†). The emission is gradually decreased in the interior of the crystal (Fig. S5D†). The fracture surface of the A3MN single crystal can also be generated by cracking with tweezers and the edge of the defect area becomes much emissive than the inner part of the crystal, as observed using the confocal microscope (Fig. 8A). The relative fluorescence intensity is plotted in Fig. 8C; the two sharp peaks indicate strong emission from the fracture surfaces in the edges of the single crystal.

The above experiments show that the intact single crystal of A3MN is weakly emissive while the defect area on the crystal exhibits intense fluorescence. The antiparallel face-to-face packing mode in the crystal lattice suggests the existence of strong π–π interactions, resulting in the weak emission. This packing mode is similar to that observed in many conventional ACQ systems bearing large flat disk-like conjugation planes. Nevertheless, different from typical ACQ molecules like pyrene or perylene, there are rotatable single bonds in the disk-like plane of A3MN. Once exogenic force is applied on the crystal, the regular face-to-face packing and the consequent strong π–π stacking may be damaged. As a result, the A3MN molecules have to adjust their conformation by intramolecular rotation to a right angle. When adopting a twisted conformation, the molecules can no longer experience strong π–π interactions and the fluorescence can thus be turned on.

Mechanochromic luminescence

Mechanochromic luminogens, which change their fluorescence properties in response to external stimuli, have attracted considerable interest over the past decades.[23] These materials can potentially be used as sensors,[24] memory chips,[25] and security inks.[26] Previously, AIE/AEE materials have been found to show mechanochromism upon the transition of crystalline and amorphous states under external stimuli.[19c,d] In most cases, upon applying mechanical force, a bathochromic shift in emission colours and a decrease in fluorescence intensity can be observed. Mechanochromic luminogens showing turn-on properties are still rarely reported. In principle, mechanical force which can cause crystal defects can induce the emission of A3MN, which could be a representative turn-on mechanochromic luminogen.

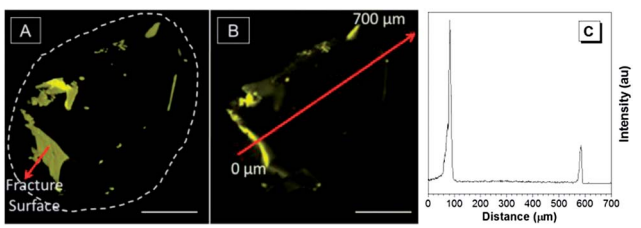

Fig. 8 (A) 3D photo and (B) one single internal monolayer of the A3MN single crystal with a fracture surface. Scale bar: 200 μm. (E) Fluorescence intensity of a single crystal of A3MN along the direction of the arrow in picture B.

To verify this hypothesis, we apply external forces, such as grinding and hitting to the crystal. As shown in Fig. 9A, the emission spectrum of the pristine A3MN crystal is nearly a flat line parallel to the abscissa; after grinding, A3MN becomes highly fluorescent with an emission peak at 563 nm. The change of the fluorescence can be clearly seen from the photographs taken under UV illumination (Fig. 9C). The single crystal shows weak red emission. After grinding or hitting by a glass rod, powders with bright yellow emission are observed with the Φ_F value as high as 48.8% and a decay lifetime of 5.99 ns (Fig. S6†). A short video was made to demonstrate the remarkable fluorescence response of the crystal to mechanical force.

Quantitative experiments are carried out by using a needle to apply mechanical force on the A3MN crystal surface. The pricked area, where defects are formed, becomes emissive (Fig. 10A). Relative intensity is recorded using a fluorescence microscope and shown in Fig. 10B. The intensity in the pricked area (>104 au) is much higher than that of the intact surface (<42 au). The fluorescence intensity is proportional to the force applied to generate the defects. Pressure lower than 0.08 N does not cause an obvious change on the emission intensity (Fig. 10C). When the pressure reaches 0.1 Newton, the emission intensity is greatly increased. Further enhancing the force leads to the gradual increase of the fluorescence intensity, which demonstrates the possibility of using A3MN crystals for quantitative analysis of mechanical force in a micro area.

Ultrasound-induced emission

Ultrasound has been used in many different fields such as object detection (sonar), ultrasonic imaging (sonography) and distance measurement. Ultrasound-related techniques have been making great contribution to a wide range of areas from national defence, scientific research, clinical diagnosis to many other aspects of the daily life of humans. For most ultrasonic

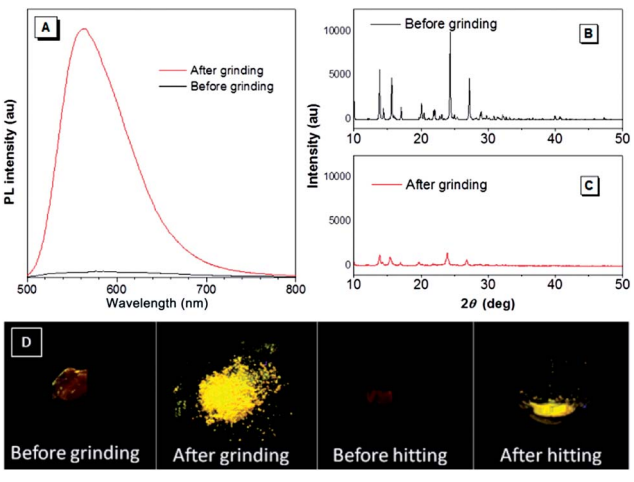

Fig. 9 (A) PL spectra of a single crystal of A3MN before and after grinding. Excitation wavelength: 445 nm. (B and C) XRD diffractograms of (B) the intact single crystal and (C) ground crystal. (D) Photograph of a single crystal of A3MN before and after grinding/hitting taken under UV irradiation from a hand-held UV lamp.

 This journal is © The Royal Society of Chemistry 2013

Published on 24 September 2013. Downloaded by HK University of Science and Technology on 01/09/2017 07:53:27.

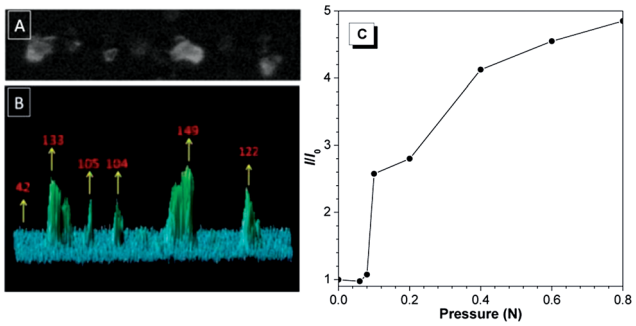

Fig. 10 (A) Defect areas on the crystal of A3MN made by mechanical pricking with a needle. (B) 3D surface plot showing the relative peak intensities of the defect areas shown in panel A. (C) Change in relative emission intensity (I/I_0) of the pricked area *versus* the force applied.

devices, the core technology is signal transformation, in other words, translation of the ultrasonic signal to the optical or electronic signals that can be easily recognized. Ultrasound-induced emission, which translates the ultrasonic signals to fluorescence signals, has aroused much research attention.[27] Previous studies have reported the phenomenon of ultrasound-induced emission, in which the ultrasound attack changes the supramolecular self-assembly or the construction of an organogel.[28] Since A3MN is defect sensitive and ultrasound attack is another method to create the defect, we propose that A3MN should also possess the ultrasound-induced emission property.

To prove this idea, we expose the microcrystals of A3MN to ultrasound by ultrasonification for 1 min. The nonemissive microcrystals suspended in aqueous solution are smashed and made highly emissive, showing the ultrasound-induced emission phenomenon (Fig. 11A). The luminescent crystals at the scale of micron can be clearly seen under a fluorescence microscope (Fig. 11B).

The microcrystals of A3MN can be smashed by ultrasound and made emissive. Large crystals of A3MN can hardly be completely destroyed by ultrasound. Instead, defects on the surface of the crystals are generated. A large crystal of A3MN is immersed in water and then exposed to 40 Hz ultrasonic waves for 1 min. The original crystal emits dim light; after sonication,

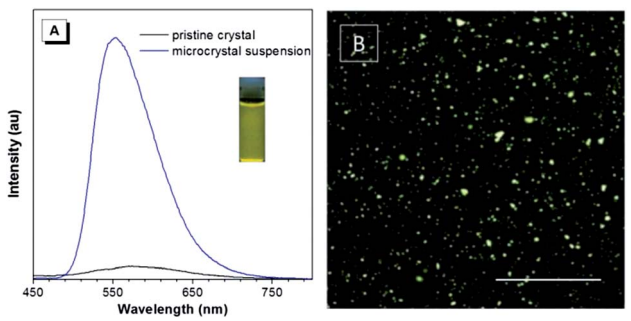

Fig. 11 (A) PL spectra of the microcrystals of A3MN before and after ultrasonication. Inset: the photograph of microcrystal suspension of A3MN after ultrasonication taken under UV illumination. (B) Fluorescence image of the fractured A3MN microcrystals. Scale bar: 50 μm. Acoustic frequency: 40 Hz.

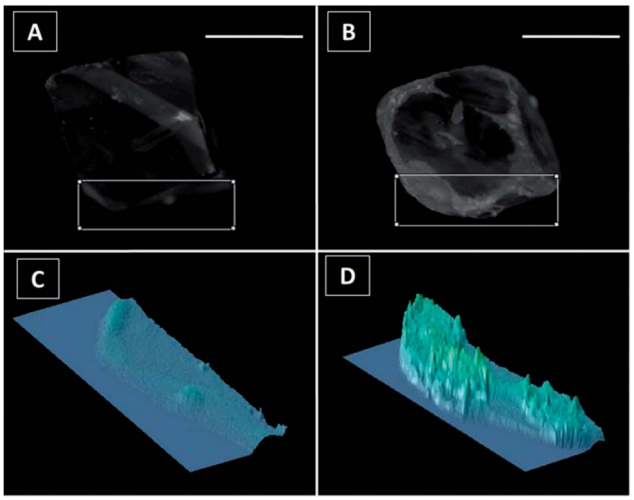

Fig. 12 Confocal micrographs of a single crystal of A3MN (A) before and (B) after attacked by ultrasonic waves. 3D surface plot of the chosen area (shown in rectangles) of the crystal: (C) before and (D) after ultrasonic attack. Scale bar: 50 μm. Excitation wavelength: 405 nm. Acoustic frequency: 40 Hz.

the edge of the crystal becomes fluorescent (Fig. 12A and B). In order to have a better comparison, surface plots of the selected area are shown in Fig. 12C and D. Fluorescence signals are depicted in altitude: the pristine crystal shows a gentle gradient (Fig. 12C), indicating the weak fluorescence, whereas the gradient become much more cliffy, indicating the strong fluorescence upon attack by ultrasonic waves. This observation further demonstrates the ultrasound-induced emission property of A3MN crystals.

Conclusions

In summary, we have designed and synthesized a new aggregation-enhanced emission luminogen, A3MN, and investigated its photophysical properties. With strong donor and acceptor moieties in its simple structure, A3MN experiences solvatochromism with a bathochromic shift in polar solvents. Because of the strong intermolecular π–π stacking, the crystals of A3MN are weakly fluorescent. Interestingly, in the defect area on the surface of the crystal, strong yellow emission can be observed. The defect-sensitive emission can be triggered by applying mechanical forces with a detection limit as low as 0.1 Newton or exposure to ultrasonic waves. Such defect-sensitive luminescent materials are promising candidates to be used in security, anti-theft and trace inspection.

Acknowledgements

The work was partially supported by the National Basic Research Program of China (973 Program; 2013CB834701), the National Science Foundation of China (20974028, 51073026, 51061160500, and 21074011), the Research Grants Council of Hong Kong (604711, 602212, HKUST2/CRF/10 and N_HKUST620/11), and the University Grants Committee of Hong Kong (AoE/P-03/08), the Specialized Research Fund for the Doctoral Program of Higher

Published on 24 September 2013. Downloaded by HK University of Science and Technology on 01/09/2017 07:53:27.

Education 35 (Grant no. 20091101110031), and the Major Project Seed Research Program of Beijing Institute of Technology (Grant no. 2012CX01008). B. Z. Tang thanks the support of the Guangdong Innovative Research Team Program of China (201101C0105067115).

Notes and references

1 (*a*) *Advanced Concepts in Fluorescence Sensing*, ed. C. D. Geddes and J. R. Lakopwicz, Springer, Norwell, 2005; (*b*) E. A. Jares-Erijman and T. M. Jovin, *Nat. Biotechnol.*, 2003, **21**, 1387; (*c*) H. Saigusa and E. C. Lim, *J. Phys. Chem.*, 1995, **99**, 15738.

2 C. W. Tang and S. A. Vanslyke, *Appl. Phys. Lett.*, 1987, **51**, 913.

3 S. R. Mujumdar, R. B. Mujumdar, C. M. Grant and A. S. Waggoner, *Bioconjugate Chem.*, 1996, **7**, 356.

4 (*a*) J. S. Yang and J. L. Yan, *Chem. Commun.*, 2008, 1501; (*b*) C. W. Wu, C. M. Tsai and H. C. Lin, *Macromolecules*, 2006, **39**, 4298; (*c*) F. He, Y. Tang, S. Wang, Y. Li and D. Zhu, *J. Am. Chem. Soc.*, 2005, **127**, 12343; (*d*) S. Hecht and J. M. J. Frechet, *Angew. Chem., Int. Ed.*, 2001, **40**, 74; (*e*) B. S. Gaylord, S. Wang, A. J. Heeger and G. C. Bazan, *J. Am. Chem. Soc.*, 2001, **123**, 6417; (*f*) P. N. Taylor, M. J. O'Connell, L. A. McNeill, M. J. Hall, R. T. Aplin and H. L. Anderson, *Angew. Chem., Int. Ed.*, 2000, **39**, 3456.

5 (*a*) J. Luo, Z. Xie, J. W. Y. Lam, L. Cheng, H. Chen, C. Qiu, H. S. Kwok, X. Zhan, Y. Liu, D. Zhu and B. Z. Tang, *Chem. Commun.*, 2001, 1740; (*b*) B. Z. Tang, X. Zhan, G. Yu, P. P. S. Lee, Y. Liu and D. Zhu, *J. Mater. Chem.*, 2001, **11**, 2974.

6 Y. Dong, J. W. Y. Lam, A. Qin, J. Sun, J. Liu, Z. Li, J. Sun, H. H. Y. Sung, I. D. Williams, H. S. Kwok and B. Z. Tang, *Chem. Commun.*, 2007, 3255.

7 (*a*) G. Yu, S. Yin, Y. Liu, J. Chen, X. Xu, X. Sun, D. Ma, X. Zhan, Q. Peng, Z. Shuai, B. Z. Tang, D. Zhu, W. Fang and Y. Luo, *J. Am. Chem. Soc.*, 2005, **127**, 6335; (*b*) K. Li, W. Qin, D. Ding, J. Geng, J. Liu, X. Zhang, H. Liu, B. Liu and B. Z. Tang, *Sci. Rep.*, 2013, **3**, 1150.

8 C. Allain, S. R. Lartia, G. Bordeau, F. D. F. Charra, P. Tauc and M. T. Fichou, *ChemBioChem*, 2007, **8**, 424.

9 Z. Zhao, J. W. Y. Lam and B. Z. Tang, *J. Mater. Chem.*, 2012, **22**, 23726.

10 Y. T. Wu, M. Y. Kuo, Y. T. Chang, C. C. Shin, T. C. Wu, C. C. Tai, T. H. Cheng and W. S. Liu, *Angew. Chem., Int. Ed.*, 2008, **47**, 9891.

11 Z. Wang, H. Shao, J. Ye, L. Tang and P. Lu, *J. Phys. Chem. B*, 2005, **109**, 19627.

12 C. X. Yuan, X. T. Tao, L. Wang, J. X. Yang and M. H. Jiang, *J. Phys. Chem. C*, 2009, **113**, 6809.

13 K. Shiraishi, T. Kashiwabara, T. Sanji and M. Tanaka, *New J. Chem.*, 2009, **33**, 1680.

14 G. Qian, B. Dai, M. Luo, D. Yu, J. Zhan, Z. Zhang, M. Dongge and Z. Y. Wang, *Chem. Mater.*, 2008, **20**, 6208.

15 X. Feng, B. Tong, J. B. Shen, J. B. Shi, T. Y. Han, L. Chen, J. G. Zhi, P. Lu, Y. G. Ma and Y. P. Dong, *J. Phys. Chem. B*, 2010, **114**, 16731.

16 Z. R. Grabowski and K. Rotkiewicz, *Chem. Rev.*, 2003, **103**, 3899.

17 (*a*) Y. Hong, J. W. Y. Lam and B. Z. Tang, *Chem. Soc. Rev.*, 2011, **40**, 5361; (*b*) Y. Hong, J. W. Y. Lam and B. Z. Tang, *Chem. Commun.*, 2009, 4332.

18 (*a*) A. Leino and B. M. Loo, *Ann. Clin. Biochem.*, 2007, **44**, 563; (*b*) W. Putalun, H. Tanaka and Y. Shoyama, *Phytochem. Anal.*, 2005, **16**, 370.

19 (*a*) Y. Dong, J. W. Y. Lam, A. Qin, J. Liu, Z. Li, B. Z. Tang, J. Sun and H. S. Kwok, *Appl. Phys. Lett.*, 2007, **91**, 011111; (*b*) J. Liu, Y. Zhong, P. Lu, Y. Hong, J. W. Y. Lam, M. Faisal, Y. Yu, K. S. Wong and B. Z. Tang, *Polym. Chem.*, 2010, **1**, 426; (*c*) Y. Dong, B. Xu, J. Zhang, X. Tan, L. Wang, J. Chen, H. Lv, S. Wen, B. Li, L. Ye, B. Zou and W. Tian, *Angew. Chem.*, 2012, **124**, 10940; (*d*) H. Li, X. Zhang, Z. Chi, B. Xu, W. Zhou, S. Liu, Y. Zhang and J. Xu, *Org. Lett.*, 2011, **13**, 556.

20 (*a*) J. C. Sanchez and W. C. Trogler, *J. Mater. Chem.*, 2008, **18**, 3143; (*b*) E. L. Que, D. W. Domaille and C. J. Chang, *Chem. Rev.*, 2008, **108**, 1517; (*c*) M. Sameiro and T. Goncalves, *Chem. Rev.*, 2009, **109**, 190.

21 Y. Liu, Y. Yu, J. W. Y. Lam, Y. Hong, M. Faisal, W. Z. Yuan and B. Z. Tang, *Chem.–Eur. J.*, 2010, **16**, 8433.

22 (*a*) M. Liong, J. Lu, M. Kovochich, T. Xia, S. G. Ruehm, A. E. Nel, F. Tamanoi and J. I. Zink, *ACS Nano*, 2008, **2**, 889; (*b*) Y. H. Deng, D. W. Qi, C. H. Deng, X. M. Zhang and D. Y. Zhao, *J. Am. Chem. Soc.*, 2008, **130**, 28; (*c*) A. Aboshi, N. Kurumoto, T. Yamada and T. Uchino, *J. Phys. Chem. C*, 2007, **111**, 8483; (*d*) G. Vaccaro, S. Agnello, G. Buscarino, M. Cannas and L. Vaccaro, *J. Non-Cryst. Solids*, 2011, **357**, 1941; (*e*) L. Vaccaro, A. Morana, V. Radzig and M. Cannas, *J. Phys. Chem. C*, 2011, **115**, 19476.

23 Z. Chi, X. Zhang, B. Xu, X. Zhou, C. Ma, Y. Zhang, S. Liu and J. Xu, *Chem. Soc. Rev.*, 2012, **41**, 3878.

24 (*a*) Z. Ning, Z. Chen, Q. Zhang, Y. Yan, S. Qian, Y. Cao and H. Tian, *Adv. Funct. Mater.*, 2007, **17**, 3799; (*b*) B. R. Crenshaw, M. Burnworth, D. Khariwala, A. Hiltner, P. T. Mather, R. Simha and C. Weder, *Macromolecules*, 2007, **40**, 2400; (*c*) M. Kinami, B. R. Crenshaw and C. Weder, *Chem. Mater.*, 2006, **18**, 946; (*d*) A. Pucci, F. D. Cuia, F. Signori and G. Ruggeri, *J. Mater. Chem.*, 2007, **17**, 783.

25 (*a*) S. Hirata and T. Watanabe, *Adv. Mater.*, 2006, **18**, 2725; (*b*) C. E. Olson, M. J. R. Previte and J. T. Fourkas, *Nat. Mater.*, 2002, **1**, 225; (*c*) M. Irie, T. Fukaminato, T. Sasaki, N. Tamai and T. Kawai, *Nature*, 2002, **420**, 759.

26 A. Kishimura, T. Yamashita, K. Yamaguchi and T. Aida, *Nat. Mater.*, 2005, **4**, 546.

27 (*a*) E. G. Schutt, D. H. Klein, R. M. Mattrey and J. G. Riess, *Angew. Chem., Int. Ed.*, 2003, **42**, 3218; (*b*) G. J. Price, M. Ashokkumar and F. Grieser, *J. Am. Chem. Soc.*, 2004, **126**, 2755; (*c*) C. Dou, D. Chen, J. Iqbal, Y. Yuan, H. Zhang and Y. Wang, *Langmuir*, 2011, **27**, 6323.

28 N. Komiya, T. Muraoka, M. Iida, M. Miyanaga, K. Takahashi and T. Naota, *J. Am. Chem. Soc.*, 2011, **133**, 16054.

 This journal is © The Royal Society of Chemistry 2013